

# Crystal-field potential and short-range order effects in inelastic neutron scattering, magnetization, and heat capacity of the cage-glass compound HoB<sub>12</sub>

B. Z. Malkin<sup>1</sup>, E. A. Goremychkin<sup>2</sup>, K. Siemensmeyer<sup>3</sup>, S. Gabáni<sup>4</sup>, K. Flachbart<sup>4</sup>, M. Rajňák<sup>4</sup>,  
A. L. Khoroshilov<sup>5</sup>, K. M. Krasikov<sup>5</sup>, N. Yu. Shitsevalova<sup>6</sup>, V. B. Filipov<sup>6</sup>, and N. E. Sluchanko<sup>5,\*</sup>

<sup>1</sup>Kazan Federal University, Theoretical Physics Department, 420008 Kazan, Russia

<sup>2</sup>Frank Laboratory of Neutron Physics, Joint Institute for Nuclear Research, Joliot-Curie 6, Dubna, 141980 Moscow reg., Russia

<sup>3</sup>Helmholtz Zentrum Berlin, D-14109 Berlin, Germany

<sup>4</sup>Institute of Experimental Physics SAS, Watsonova 47, 04001 Košice, Slovakia

<sup>5</sup>Prokhorov General Physics Institute of Russian Academy of Sciences, Vavilova 38, 119991 Moscow, Russia

<sup>6</sup>Frantsevich Institute for Problems of Materials Science, NASU, Krzhynanovskyy str., 3, 03142 Kyiv, Ukraine



(Received 19 June 2021; revised 7 October 2021; accepted 19 October 2021; published 29 October 2021)

The strongly correlated system Ho<sup>11</sup>B<sub>12</sub> with boron sublattice Jahn-Teller instability and nanoscale electronic phase separation (dynamic charge stripes) was studied in detail by inelastic neutron scattering (INS), magnetometry, and heat capacity measurements at temperatures in the range of 3–300 K. From the analysis of registered INS spectra, we determined parameters of the cubic crystal field (CF) at holmium sites  $B_4 = -0.333$  meV and  $B_6 = -2.003$  meV (in Stevens notations), with an unconventional large ratio  $B_6/B_4$  pointing to the dominant role of conduction electrons in the formation of a CF potential. The molecular field in the antiferromagnetic (AFM) state  $B_{\text{loc}} = (1.75 \pm 0.1)$  T has been directly determined from the INS spectra together with short-range order effects detected in the paramagnetic state. A comparison of measured magnetization in diluted Lu<sub>0.99</sub>Ho<sub>0.01</sub>B<sub>12</sub> and concentrated HoB<sub>12</sub> single crystals showed a strong suppression of Ho magnetic moments by AFM exchange interactions in holmium dodecaboride. To account explicitly for the short-range AFM correlations, a self-consistent holmium dimer model was developed that allowed us to reproduce successfully field and temperature variations of the magnetization and heat capacity in the cage-glass phase of HoB<sub>12</sub> in external magnetic fields.

DOI: [10.1103/PhysRevB.104.134436](https://doi.org/10.1103/PhysRevB.104.134436)

## I. INTRODUCTION

Rare earth (RE) dodecaborides  $RB_{12}$  [face-centered cubic (fcc) lattice, space group  $Fm\bar{3}m$ ,  $R = \text{Tb, Dy, Ho, Er, Tm, Yb, and Lu}$ ] with a cage-glass structure [1] attract considerable attention due to a unique combination of their physical properties, including high melting temperature, microhardness, and high chemical stability [2,3]. In the antiferromagnetic (AFM)  $RB_{12}$  series, the Néel temperature decreases monotonically from TbB<sub>12</sub> ( $T_N \approx 22$  K) to TmB<sub>12</sub> ( $T_N \approx 3.2$  K) while maintaining a similar conduction band, consisting of  $5d$  ( $R$ ) and  $2p$  ( $B$ ) atomic orbitals, and changing only with the number  $n_{4f}$  of  $4f$  shell electrons of RE ions ( $8 \leq n_{4f} \leq 14$ ) [4,5]. The increase of the  $4f$  filling from  $n_{4f} = 12$  to 13 leads to dramatic changes both in magnetic and charge transport characteristics [6–8], demonstrating the transition from a AFM metal (TmB<sub>12</sub>) to a paramagnetic narrow-gap semiconductor with intermediate valence [9] of Yb ions (YbB<sub>12</sub>). Despite intensive investigations, the nature of this semiconducting state in the Kondo insulator YbB<sub>12</sub> remains a subject of active debates [10–15].

In recent studies of the charge transport, magnetic, and thermal properties and fine details of fcc crystal structure

of nonmagnetic LuB<sub>12</sub>, AFM HoB<sub>12</sub>-TmB<sub>12</sub> compounds, and solid solutions Tm<sub>1-x</sub>Yb<sub>x</sub>B<sub>12</sub>, it was established that the cooperative Jahn-Teller dynamics of B<sub>12</sub> clusters should be considered one of the main factors responsible for a strong renormalization of the quasiparticle spectra, electron phase separation, and symmetry breaking in RE dodecaborides [16–20]. It was suggested that the ferrodistorptive effect in the boron sublattice generates both collective modes (overdamped oscillators in the frequency range 250–1000 cm<sup>-1</sup> [19,20] in the dynamic conductivity spectra of each of the metallic  $RB_{12}$  compounds and rattling modes—quasilocal vibrations of heavy RE ions embedded in the oversized B<sub>24</sub> cavities. Large amplitude displacements of  $R$  ions cause (i) the development of vibrational instability at intermediate temperatures  $\sim 150$  K on reaching the Ioffe-Regel limit for a phonon localization and (ii) strong periodic changes in the hybridization of atomic  $5d$  ( $R$ ) and  $2p$  ( $B$ ) orbitals, altering their overlap. Accordingly, these overlap alterations along the rhombic (of [110] type) axes are responsible for the modulation of the conduction electron density with a frequency  $\sim 2 \times 10^{11}$  Hz [19], providing the emergence of dynamic charge stripes which are the feature of a nanoscale electron instability and electron phase separation. It was argued in Refs. [19,20] that nonequilibrium charge carriers dominated in RE dodecaborides, taking 50–70% from the total number of conduction electrons. These *hot electrons* cannot participate in the indirect exchange (RKKY

\*nes@lt.gpi.ru

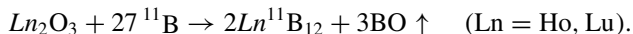
interaction) between the RE magnetic moments. Moreover, it was concluded in the studies of  $\text{HoB}_{12}$  and  $\text{Ho}_x\text{Lu}_{1-x}\text{B}_{12}$  that the suppression of the magnetic exchange interaction in nano-sized filamentary structures should be considered as the main sequence of the electron instability, providing a symmetry lowering and formation of Maltese crosslike phase diagrams of  $\text{RB}_{12}$  AFMs [21,22]. Because of the loosely bound state of RE ions in the rigid boron cage, there is also an order-disorder phase transition to the cage-glass state [1] at temperature  $T^* \sim 60$  K, resulting in the random displacements of RE ions from their positions in the fcc lattice. This disordering induces a formation of nano-sized clusters of RE ions (dimers, trimers, etc.) with AFM exchange, and corresponding domains (which in  $\text{HoB}_{12}$  have a form of a cigar elongated parallel to trigonal axes (of [111] type) [23]) should be considered to explain the nature of the short-range magnetic order detected in  $\text{RB}_{12}$  AFMs at temperatures far above  $T_N$ .

As with all RE systems, the interaction of  $f$  electrons with the crystal field (CF) plays a key role in determining magnetic and thermodynamic properties of RE dodecaborides. Considering that the CF potential is sensitive to structural distortions and magnetic ion displacement as well as to changes in the conduction electron density, it looks useful to investigate in detail the  $4f$  shell ground multiplet splitting in magnetic dodecaborides. Inelastic neutron scattering (INS) is the most reliable method of determining the CF potential in metallic compounds since it directly measures energies of CF excitations and intensities of magnetic dipole transitions between CF levels. In this paper, samples of  $\text{HoB}_{12}$  were used to characterize the CF potential and short-range order effects in the dodecaboride matrix by INS, magnetization, and heat capacity measurements.

## II. EXPERIMENTAL DETAILS

Since the natural mixture of boron isotopes has a high neutron absorption cross-section (767 barn), samples for INS experiments were prepared using the  $^{11}\text{B}$  isotope, whose absorption cross-section is  $\sim 0$  (0.006 barn). Along with  $\text{Ho}^{11}\text{B}_{12}$ , an isostructural compound  $\text{Lu}^{11}\text{B}_{12}$  was also synthesized. Since lutetium has fully filled the  $4f$  electronic shell and does not have a magnetic moment, the INS measurement with  $\text{Lu}^{11}\text{B}_{12}$  makes it possible to estimate the contribution of nuclear (phonon) scattering and to establish the nature of features (magnetic/nonmagnetic) in the INS spectra of  $\text{Ho}^{11}\text{B}_{12}$ .

The powder samples of  $\text{Ho}^{11}\text{B}_{12}$  and  $\text{Lu}^{11}\text{B}_{12}$  were synthesized in a two-stage process. First, the initial charges were prepared as a mixture of corresponding metal oxide ( $\text{Ln}_2\text{O}_3$ ) and isotopic boron ( $^{11}\text{B}$ ) for subsequent synthesis according to the solid-state reaction



Each mixture was pressed in the form of tablets and then was held in vacuum at 1900 K for 1 h. The tablets of synthesized dodecaborides  $\text{Ln}^{11}\text{B}_{12}$  were ground, then newly pressed and held at 2000 K for homogenization. Further, the tablets were ground in a steel mortar, and the obtained powders were treated by hot HCl acid to remove traces of Fe. X-ray phase analysis showed that the prepared powders of  $\text{Ho}^{11}\text{B}_{12}$  and  $\text{Lu}^{11}\text{B}_{12}$  were single-phase products of  $\text{UB}_{12}$ -type fcc crys-

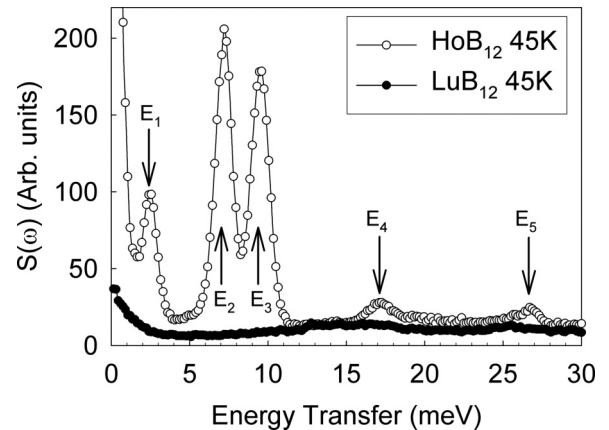


FIG. 1. Inelastic neutron scattering spectra of  $\text{Ho}^{11}\text{B}_{12}$  and  $\text{Lu}^{11}\text{B}_{12}$  measured at 45 K on NERA. The arrows show the positions of the peaks corresponding to crystal field (CF) excitations.

tal structure. These  $\text{Ln}^{11}\text{B}_{12}$  powders were prepared using isotope-enriched boron ( $^{11}\text{B}$ ; Ceradyne Inc., USA, with enrichment of 99.61 at. %, purity  $>99.96\%$ ) and metal oxides from the Federal State Research and Design Institute of Rare Metal Industry (Moscow, Russia) with the purity of initial  $\text{Ho}_2\text{O}_3$  of 99.996 and  $\text{Lu}_2\text{O}_3$  of 99.998 mass %. Neutron diffraction measurements confirmed that the samples contained no other phases.

The INS experiments were performed at the pulsed reactor IBR-2 (FLNP, JINR, Dubna, Russia) on the time-of-flight inverse geometry spectrometer NERA [24], with a final energy of 4.65 meV and energy resolution at the elastic position of 0.8 meV, and on the direct geometry spectrometer DIN 2PI [25], using incident energy of 5 meV with a resolution of 0.28 meV. The samples, weighing  $\sim 12$  g, were placed in a thin aluminum sachet and inserted into a closed-cycle cryostat for scans in the temperature range 3–300 K.

Measurements of the magnetization field dependences for the oriented single-crystalline  $\text{Ho}_{0.01}\text{Lu}_{0.99}\text{B}_{12}$  samples in magnetic fields up to 18 T and  $\text{HoB}_{12}$  in the paramagnetic phase in external magnetic fields up to 7 T directed along the tetragonal, rhombic, and trigonal symmetry axes were performed using vibrating sample magnetometer with a cryogen-free 18 T magnet (Cryogenic Limited, UK) and SQUID MPMS-7 (Quantum Design, USA) instrument, respectively.

Precise measurements of the heat capacity of  $\text{HoB}_{12}$  and  $\text{LuB}_{12}$  single-crystalline samples at temperatures in the range 1.8–300 K in magnetic fields up to 9 T directed along the [001], [110], and [111] axes were performed using the PPMS-9 (Quantum Design) instrument. The details of the growth of  $\text{Ho}_{0.01}\text{Lu}_{0.99}\text{B}_{12}$ ,  $\text{Ho}^{11}\text{B}_{12}$ , and  $\text{LuB}_{12}$  single crystals and the preparation of oriented samples are described in Refs. [1,22].

## III. INS RESULTS

Figure 1 shows the results of the INS measurement on the NERA spectrometer at temperature of 45 K for the compounds  $\text{Ho}^{11}\text{B}_{12}$  and  $\text{Lu}^{11}\text{B}_{12}$ . Comparison of  $\text{Ho}^{11}\text{B}_{12}$  with  $\text{Lu}^{11}\text{B}_{12}$  spectra demonstrates the presence of five well-defined magnetic peaks (marked by vertical arrows) due

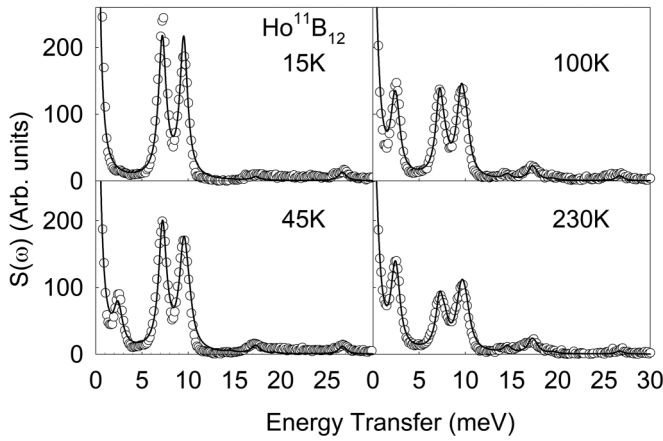


FIG. 2. Background corrected inelastic neutron scattering spectra from  $\text{Ho}^{11}\text{B}_{12}$  measured at 15, 45, 100, and 230 K on NERA. The solid lines show the profiles calculated in the framework of the crystal field (CF) model described in the text.

to transitions between CF levels at energy transfers of  $E_1 \approx 2.3$  meV,  $E_2 \approx 7.2$  meV,  $E_3 \approx 9.5$  meV,  $E_4 \approx 17.4$  meV, and  $E_5 \approx 26.7$  meV. The temperature evolution of the scattering intensities shown in Fig. 2 indicates that the intensities of peaks  $E_2, E_3, E_4$ , and  $E_5$  decrease with increasing temperature, which is a signature of transitions from the ground CF level, while the  $E_1$  peak intensity increases with increasing temperature, and therefore, this peak is associated with the transition from the excited CF level ( $E_2$ ) to the next level ( $E_3$ ). The temperature shifts of the measured energies of CF excitations in the temperature range from 15 to 230 K are rather small (the shifts of the most intensive peaks  $E_2$  and  $E_3$  do not exceed 0.15 meV). Weak temperature influence on the CF excitations correlates with the complex behavior of low-temperature thermal expansion [5] and small changes of lattice constants (of an order of  $10^{-4}$  nm) in the temperature range  $250 \text{ K} > T > T_N$  in RE dodecaborides [26,27].

Figure 3 shows the results on  $\text{Ho}^{11}\text{B}_{12}$  in the AFM state at  $T = 3.5$  K well below the Néel temperature  $T_N = 7.4$  K [20,21]. The data indicate the appearance of a new peak at energy  $E_{\text{AFM}} = 0.8$  meV and a significant shift in the energy position of peaks  $E_2$  and  $E_3$  as well as a change in their intensities. This indicates a strong influence of the magnetic order on the energy and intensity of CF transitions. It is worth noting that the  $E_{\text{AFM}}$  value coincides with the magnon energy 0.8 meV at the Brillouin zone center detected at 3.5 K in the magnon excitation spectra of  $\text{HoB}_{12}$  (see fig. 16 in Ref. [23]).

#### IV. INS DATA ANALYSIS AND CF MODEL

In the case of perfect fcc  $\text{UB}_{12}$ -type lattice of  $\text{Ho}^{11}\text{B}_{12}$ , it is expected that holmium ions occupy sites with cubic point symmetry. Neglecting interactions between  $\text{Ho}^{3+}$  ions in the paramagnetic phase, we write the  $\text{Ho}^{3+}$  single-ion Hamiltonian operating in the total space of 1001 states of the  $4f^{10}$  electronic configuration in the following form:

$$H = H_{\text{FI}} + H_Z + H_{\text{CF}}, \quad (1)$$

where  $H_{\text{FI}}$  is the free-ion Hamiltonian considered in the standard parameterized form [28] with parameters taken from Ref. [29],  $H_Z = -\mathbf{M} \cdot \mathbf{B}$  is the electronic Zeeman energy in external magnetic field  $\mathbf{B}$  [here,  $\mathbf{M} = -\mu_B \sum_n (k\mathbf{l}_n + 2\mathbf{s}_n)$  is the magnetic moment operator of a  $\text{Ho}^{3+}$  ion,  $\mu_B$  is the Bohr magneton, the sum is taken over  $4f$  electrons with orbital  $\mathbf{l}_n$  and spin  $\mathbf{s}_n$  moments, respectively, and  $k$  is the orbital reduction factor], and

$$H_{\text{CF}} = 8B_4 \left\{ C_0^{(4)} + \left( \frac{5}{14} \right)^{1/2} [C_4^{(4)} + C_{-4}^{(4)}] \right\} + 16B_6 \left\{ C_0^{(6)} - \left( \frac{7}{2} \right)^{1/2} [C_4^{(6)} + C_{-4}^{(6)}] \right\} \quad (2)$$

is the CF Hamiltonian determined by phenomenological CF parameters  $B_4$  and  $B_6$  (here,  $C_n^{(m)}$  are spherical tensor operators which can be transformed to Stevens operators  $O_m^n(\mathbf{J})$

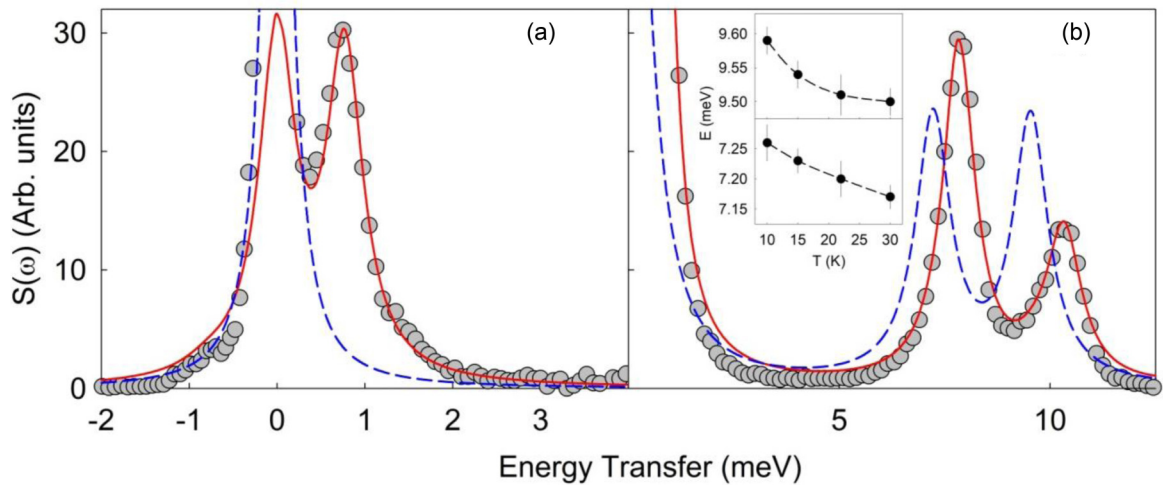


FIG. 3. Background corrected inelastic neutron scattering spectra of  $\text{Ho}^{11}\text{B}_{12}$  measured at 3.5 K for (A) energies of incident neutrons of 5 meV on DIN 2PI and (B) registered energies of 4.65 meV on NERA. The red solid line shows the profile of the crystal field (CF) + molecular field (MF) model described in the text. The blue dashed line represents the CF spectrum only. Inset shows the energy shift of the CF peaks below 30 K.

TABLE I. Measured and calculated energies (meV) of CF sublevels of the ground multiplet  $^5I_8$  of  $\text{Ho}^{3+}$  ions in  $\text{Ho}^{11}\text{B}_{12}$  and the widths  $\Delta_{\text{HF}}$  (meV) of hyperfine splittings of corresponding sublevels.

Symmetry and degeneracy	$E_i(T > T_N)$		$\Delta_{\text{HF}}$ Theory	CF excitations in INS at 3.5 K	
	Experiment	Theory		Experiment	Theory
$\Gamma_5^{(1)} 3$	0	0	0.216	0 and 0.8	0 and 0.83
$\Gamma_3^{(1)} 2$	7.2	7.18	0.005	8.0	7.94
$\Gamma_4^{(1)} 3$	9.5	9.52	0.017	11.0	10.39
$\Gamma_1 1$	–	12.30	0.004	–	–
$\Gamma_5^{(2)} 3$	17.4	17.28	0.192	18.5	18.69
$\Gamma_4^{(2)} 3$	26.7	26.58	0.152	26.8	26.62
$\Gamma_3^{(2)} 2$	–	27.05	0.042	–	–

with the reduced matrix elements  $\alpha_J, \beta_J, \gamma_J$  in a truncated basis of eigenfunctions  $|J, J_z\rangle$  of the angular momentum  $J$ ;  $C_0^{(4)} = \beta_J O_4^0/8$  and  $C_0^{(6)} = \gamma_J O_6^0/16$  [30]). When studying scattering of slow neutrons and magnetic and thermal properties of a holmium compound, we may limit ourselves by considering only the ground multiplet  $^5I_8$  of the  $4f^{10}$  electronic shell (the first excited multiplet  $^5I_7$  has an energy exceeding 7000 K). The  $^5I_8$  multiplet is split by CF of cubic symmetry into seven sublevels, four triplets, two doublets, and one singlet.

The intensity of INS in a powder sample at temperature  $T$  corresponding to magnetic dipole transitions between CF levels with the energy transfer  $\hbar\omega$  and the scattering vector  $\mathbf{Q}$  is given by the following expression [31]:

$$S(\mathbf{Q}, \omega) \propto |f(\mathbf{Q})|^2 \sum_{i,j>i} \rho_i(T) \times \sum_{\alpha=x,y,z} |(j|M_\alpha|i)|^2 F(\omega - \omega_{ji}, \Gamma_{ji}), \quad (3)$$

where  $f(\mathbf{Q})$  is the  $f$ -electron form factor,  $\rho_i(T) = \exp(-E_i/k_B T) / \sum_j \exp(-E_j/k_B T)$  (here,  $k_B$  is the Boltzmann constant) is the occupation probability of the CF level  $|i\rangle$  with the energy  $E_i$ , and  $F(\omega - \omega_{ji}, \Gamma_{ji})$  is the line shape with a half-width  $\Gamma_{ji}$ . In this paper, the Lorentzian function has been used.

In our INS data, we observed two strong transitions at the energies near  $E_2 = 7.2$  meV and  $E_3 = 9.5$  meV. The temperature evolution of their intensities indicates that they are due to transitions between the ground state and the first and second excited CF levels, correspondingly. From the fitting of observed scattering profiles under the condition of  $E_3/E_2 \approx 1.32$  and by making use of the setup resolution of 0.8 meV as a starting value of the half-width  $\Gamma_{ji}$  for all transitions, we obtained CF parameters  $B_4 = (-0.333 \pm 0.012)$  meV and  $B_6 = (-2.003 \pm 0.023)$  meV. These values of CF parameters allowed us to successfully reproduce the experimental INS spectra at 15, 45, 100, and 230 K; solid lines in Fig. 2 represent the results of the profile refinements of magnetic scattering using slightly varied half-widths (mainly increasing with the energy transfer) for different transitions. The model describes well the evolution with temperature of all the transitions. There are a few minor discrepancies between the calculated and measured spectra, although the overall agreement is very good for the CF-only model. The calculated energies of CF

sublevels of the ground multiplet and corresponding irreducible representations of the point symmetry  $O_h$  group are presented in Table I. The energy spectrum of the ground state, the  $\Gamma_5$  triplet, in an external magnetic field  $\mathbf{B}$  can be described by the effective spin Hamiltonian ( $S = 1$ ) with the isotropic  $g$  factor  $H_S = g\mu_B \mathbf{S} \cdot \mathbf{B}$ .

Holmium has only one stable isotope  $^{165}\text{Ho}$  with the nuclear spin  $I = \frac{7}{2}$ . By making use of the numerical diagonalization of the projection of the Hamiltonian in Eq. (1) on the space of 136 electron-nuclear states  $|J, I, J_z, I_z\rangle$  of the ground multiplet with added magnetic dipole hyperfine interaction  $H_{\text{HF}} = A\mathbf{J} \cdot \mathbf{I}$  (here, the hyperfine coupling constant  $A = 3.3 \times 10^{-3}$  meV [32]), we calculated the widths  $\Delta_{\text{HF}}$  of hyperfine structures of CF sublevels presented in Table I. It is seen that these widths are remarkably smaller than the INS spectrometer resolution, and we obtain practically the same scattering profiles from calculations where the hyperfine interaction is added to the single-ion Hamiltonian.

Additionally, from the data obtained, we can conclude about slight energy changes with temperature of the  $E_2$  and  $E_3$  peaks. Indeed, within the limits of experimental accuracy, the increase of  $E_2(T)$  and  $E_3(T)$  with decreasing temperature is well evident below 30 K (see inset in Fig. 3). It is worth noting that, in recent measurements of electron paramagnetic resonance (EPR) in  $\text{Ho}_x\text{Lu}_{1-x}\text{B}_{12}$  [33], strong and simultaneous changes of both the  $g$  factor ( $g = 4.1\text{--}4.8$ ) and the line width ( $\Delta B = 0.35\text{--}0.9$  T) have been observed in  $\text{HoB}_{12}$  at temperatures between 7.5 and 30 K. This result was discussed by the authors of Ref. [33] in terms of short-range AFM clusters which were observed in the paramagnetic state of  $\text{HoB}_{12}$  well above the Néel temperature  $T_N = 7.4$  K. Diffuse neutron scattering also demonstrates the presence of the short-range order reflexes in  $\text{HoB}_{12}$  at temperatures at least up to  $3T_N$  [23]. The energy shift of the CF peaks below 30 K (see inset in Fig. 3) could be also attributed to the occurrence of weak internal inhomogeneous molecular field (MF) due to short-range magnetic order.

The influence of AFM ordering on the excitation spectrum has been considered in the MF approximation with Zeeman energy  $H_Z = \pm g_J \mu_B \mathbf{J} \cdot \mathbf{B}_{\text{loc}}$  ( $\mathbf{B}_{\text{loc}}$  is the staggered local magnetic field affecting  $\text{Ho}^{3+}$  ions in AFM coupled dimers considered below) in the right-hand side of Eq. (1) when considering the magnetically ordered phase.

The MF in the AFM state has been determined directly by fitting the INS spectra measured on NERA and DIN 2PI

spectrometers at 3.5 K, assuming that the CF parameters are the same as in the paramagnetic phase. The best fit is obtained with  $B_{\text{loc}} = (1.75 \pm 0.1)$  T, and in Fig. 3, the CF + MF model describes very well the INS experimental data at both instruments. The measured and simulated values of excitation energies at 3.5 K are given in Table I.

The CF parameters in  $\text{HoB}_{12}$ , determined in this paper, have the same signs as the ones determined in  $\text{Yb}_{0.9}\text{Er}_{0.1}\text{B}_{12}$  [34] for  $\text{Er}^{+3}$  ions ( $B_4 = -1.036 \pm 0.721$  meV and  $B_6 = -1.932$  meV) and in  $\text{Lu}_{1-x}\text{Tm}_x\text{B}_{12}$  and  $\text{Yb}_{1-x}\text{Tm}_x\text{B}_{12}$  for  $\text{Tm}^{+3}$  ions ( $B_4 = -0.597$  meV and  $B_6 = -2.163$  meV) [35], but contrary to the parameter  $B_6$  that demonstrates rather weak relative changes along the lanthanide series in  $\text{RB}_{12}$ , the absolute value of the parameter  $B_4$  increases remarkably with the increasing number of  $4f$  electrons. We would like to note a specific feature of the sets of CF parameters in dodecaborides with unconventional large ratios  $B_6/B_4$  which may evidence dominant contributions into the CF potential from conduction electrons with an  $f$ -type space distribution (corresponding to the orbital moment  $l = 3$ ) in the vicinity of RE ions.

In this paper, we demonstrate the importance of accounting for  $J$ -mixing effects due to spin-orbit and CF interactions even in the case of a well-isolated multiplet of a RE ion, especially for estimations of CF parameters with small absolute values. We found it possible to obtain practically the same CF energies and INS profiles using the three-time diminished parameter  $B_4$  (but only an 8% smaller parameter  $B_6$ ) in the CF Hamiltonian defined in the truncated basis of states of the  $^5I_8$  multiplet that seems doubtful.

A possible reason for specific features of the CF parameters and their dependence on the RE ion in borides may be the local polarization of conduction electrons and, consequently, a change of the conduction electron contribution to the CF potential [36]. We plan to conduct systematic high-precision measurements of the CF parameters along the series of  $\text{RB}_{12}$  compounds to verify this assumption.

## V. MAGNETIZATION AND HEAT CAPACITY RESULTS AND ANALYSIS

The calculated value of the  $g$  factor in the spin Hamiltonian of the  $\Gamma_5^{(1)}$  ground triplet  $g = 5.56$  in the absence of the orbital reduction ( $k = 1$ ) exceeds remarkably the  $g$  factors measured in EPR experiments [33], varying with temperature from 4.8 (30 K) to 4.1 (7.5 K). Also, a substantial systematic decrease of the magnetization was unveiled by the magnetometry of the concentration series of isostructural  $\text{Ho}_x\text{Lu}_{1-x}\text{B}_{12}$  single crystals with the increasing concentration of  $\text{Ho}^{3+}$  ions  $x = 0.01, 0.04, 0.1, 0.2, 0.3, 0.5,$  and 1 (not shown) [37]. We consider here both single-ion and collective mechanisms of the magnetic moment reduction in RE dodecaborides. First, the orbital magnetic moment of a localized  $4f$  electron is reduced due to the hybridization of its wave functions with the wave functions of conduction electrons. Additional reduction of the effective magnetic moment can be induced by low-symmetry components of the CF generated by random lattice strains which compete with the magnetic field because of different symmetry relative to the time inversion. This effect is important at low temperatures when energies  $k_B T$  of ther-

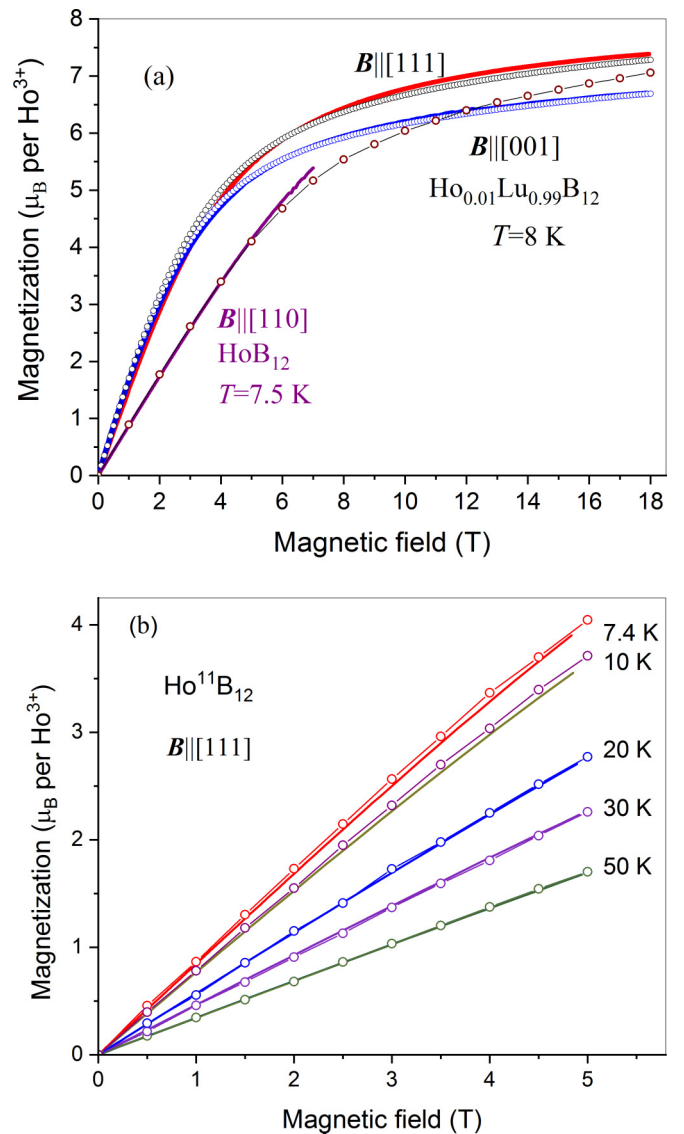


FIG. 4. Measured (solid lines) and calculated (symbols) magnetization of (a)  $\text{Ho}_{0.01}\text{Lu}_{0.99}\text{B}_{12}$  (for a direct comparison, the measured magnetization of the concentrated system  $\text{HoB}_{12}$  is also shown) and (b)  $\text{Ho}^{11}\text{B}_{12}$  single crystals in magnetic fields  $B \parallel [111]$  at temperatures 7.4, 10, 20, 30, and 50 K.

mal excitations are comparable with random splittings of the degenerate ground state of a RE ion [38]. The hybridization of wave functions can be accounted for by introduction of the orbital reduction factor  $k < 1$ . We found it possible to reproduce successfully the measured field dependences of magnetization  $\mathbf{M}(\mathbf{B})$  of the diluted system  $\text{Ho}_{0.01}\text{Lu}_{0.99}\text{B}_{12}$  in magnetic fields up to 18 T directed along the  $[111]$ ,  $[110]$ , and  $[001]$  axes at 8 K in the framework of the CF model derived above by making use of the orbital reduction factor  $k = 0.91$  [see Fig. 4(a)]. Note, the CF model is in agreement with the observed cubic magnetic anisotropy [23],  $M(\mathbf{B} \parallel [111]) \approx M(\mathbf{B} \parallel [110]) > M(\mathbf{B} \parallel [001])$  that becomes pronounced in the fields  $B > 3$  T.

In the magnetically concentrated system  $\text{HoB}_{12}$ , magnetic interactions between  $\text{Ho}^{3+}$  ions play the dominant role in the suppression of effective magnetic moments and formation of

specific features of the magnetization field and temperature dependencies, such as the linear dependence on the field strength and no signs of the saturation or magnetic anisotropy in the fields up to 4.5 T [see Fig. 4(b)]. The concrete magnetic structure in HoB<sub>12</sub> at temperatures below  $T_N$  is still unknown (see discussion in Ref. [23]), and to account explicitly for the short-range AFM correlations, we consider a minimal cluster model, an exchange-coupled holmium dimer in self-consistent MF  $\mathbf{B}_{MF} = -\lambda \langle \mathbf{M} \rangle$  (here,  $\langle \mathbf{M} \rangle$  is the average holmium magnetic moment in external magnetic field in the paramagnetic phase, and  $\lambda$  is the MF constant linear in the corresponding exchange integral) originating from interdimer interactions. Note a strong reduction of the magnetization of RE dimers allocated by the ladder space structure was revealed in RE higher borides  $RB_{50}$  (see Refs. [39,40] and references therein). The Hamiltonian of a dimer determined in the space of  $17 \times 17$  states corresponding to the CF sublevels of the ground multiplets of a pair of holmium ions has the following form:

$$H_D = H_1 + H_2 - J_{ex} \mathbf{S}_1 \cdot \mathbf{S}_2 - (\mathbf{M}_1 + \mathbf{M}_2) \cdot \mathbf{B}_{MF}, \quad (4)$$

where  $\mathbf{S}_i$  and  $\mathbf{M}_i$  ( $i = 1, 2$ ) are operators of the total spin moment and magnetic moment of a Ho<sup>3+</sup> ion, and  $H_i$  is the single-ion Hamiltonian in Eq. (1) projected on the wave functions of the <sup>5</sup>I<sub>8</sub> multiplet of the 4f<sup>10</sup> configuration. The exchange integral  $J_{ex}$  and the mean field constant  $\lambda$  are considered the fitting parameters. The average values of the magnetic moments  $\langle \mathbf{M}(\mathbf{B}) \rangle$  are solutions of the coupled self-consistent equations:

$$\langle \mathbf{M} \rangle = \frac{\text{Tr}\{(\mathbf{M}_1 + \mathbf{M}_2) \exp[-\frac{H_D(\mathbf{B}_{loc})}{k_B T}]\}}{2\text{Tr}\{\exp[-\frac{H_D(\mathbf{B}_{loc})}{k_B T}]\}}, \quad (5)$$

$$\langle \mathbf{M} \rangle = \frac{\mathbf{B}_{loc} - \mathbf{B}}{\lambda}, \quad (6)$$

where  $\mathbf{B}_{loc} = \mathbf{B} + \mathbf{B}_{MF}$ . From fitting the magnetization curve at the temperature 7.4 K [see Fig. 4(b)], we obtained  $J_{ex} = -2.55$  K and  $\lambda = -0.38$  T/ $\mu_B$  (negative signs correspond to AFM interactions), but to reproduce the experimental data at higher temperatures, we found it necessary to decrease slightly the exchange integral and, correspondingly, the parameter  $J_{ex} = -2.39$  K ( $T = 10$  K),  $-2.23$  K ( $T = 20$  K),  $-2.09$  K ( $T = 30$  K), and  $-1.92$  K ( $T = 50$  K). The results of modeling match satisfactorily the measured field dependencies of the holmium magnetic moments in the paramagnetic phase. Changes of the exchange integrals may be caused by the thermal lattice expansion or by decreasing the Ho-Ho distances in dimers with temperature lowering in the disordered cage-glass phase.

It should be noted that the calculation of profiles of INS by noninteracting dimers by making use of the CF and exchange parameters presented above brings about practically the same results as in the case of noninteracting holmium ions in the paramagnetic phase because the exchange splitting of degenerate CF sublevels does not exceed the spectral resolution of 0.8 meV.

Next, the derived models were checked by calorimetric studies of HoB<sub>12</sub> single crystals in the paramagnetic phase in external magnetic fields. Figure 5(a) shows the measured temperature dependencies of heat capacity  $C(T, B)$  in magnetic

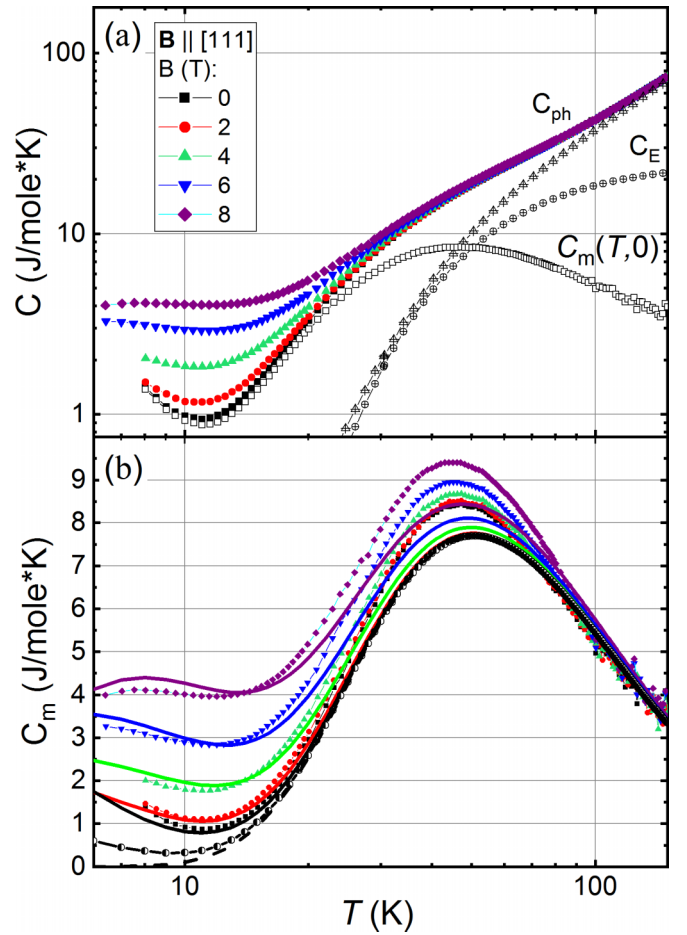


FIG. 5. (a) Temperature dependencies of specific heat  $C(T, B)$  for  $\mathbf{B} \parallel [111]$ , Einstein component  $C_E$ , phonon contribution  $C_{ph}$ , and magnetic heat capacity  $C_m(T, 0)$  of HoB<sub>12</sub>. (b) The results of  $C_m(T, B)$  modeling. Thick solid lines represent the fitting in magnetic fields  $B = 0, 2, 4, 6,$  and  $8$  T in the framework of a dimer model. The lowest dashed line and the line with circles show the calculated heat capacity in zero magnetic field for noninteracting Ho<sup>3+</sup> ions and holmium dimers (with the intradimer exchange integral  $J_{ex} = -2.55$  K determined from the analysis of the magnetization), respectively.

fields  $B = 0, 2, 4, 6,$  and  $8$  T, Einstein component  $C_E$ , phonon contribution  $C_{ph}$ , and magnetic specific heat  $C_m(T, B = 0)$ , where the last term is separated from phonon and conduction electron components by subtracting the specific heat of the nonmagnetic reference LuB<sub>12</sub> compound (see Ref. [38] for more details). Additionally, we considered the difference in Einstein temperatures of HoB<sub>12</sub> ( $\theta_E \approx 190$  K [41]) and LuB<sub>12</sub> ( $\theta_E \approx 164$  K) [1,5,38] using the following relation:

$$C_m(\text{HoB}_{12}) = [C(\text{HoB}_{12}) - C_E(\text{HoB}_{12})] - [C(\text{LuB}_{12}) - C_E(\text{LuB}_{12})], \quad (7)$$

and the well-known Einstein formula for the specific heat [1]:

$$C_E = \sum_j R \left( \frac{T_j}{T} \right)^2 \frac{\exp\left(\frac{T_j}{T}\right)}{\left[\exp\left(\frac{T_j}{T}\right) - 1\right]^2}, \quad (8)$$

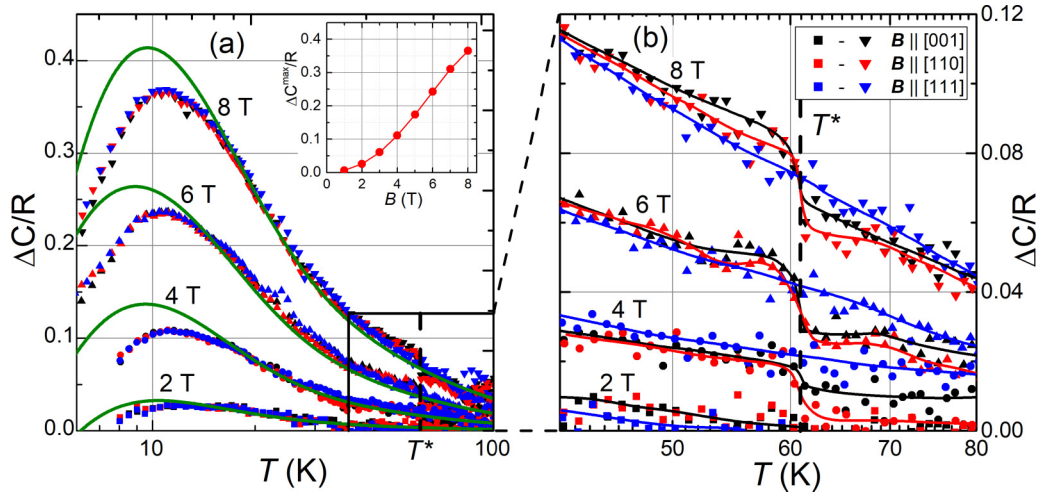


FIG. 6. (a) Measured temperature dependences of the magnetic field induced difference  $\Delta C = C(T, B) - C(T, 0)$  for  $\mathbf{B} \parallel [001]$ ,  $\mathbf{B} \parallel [110]$ , and  $\mathbf{B} \parallel [111]$  configurations (symbols) in  $\text{HoB}_{12}$ . Solid lines correspond to the results of simulations. Inset shows the magnetic field dependence of the  $\Delta C$  maximum. (b) Large scale plot of  $\Delta C(T, B)$  in the temperature range 40–80 K.  $T^*$  denotes the cage-glass transition anomaly.

where  $R$  is the gas constant,  $T_j = \hbar\omega_j/k_B$ , and the sum is taken over Einstein phonons with frequencies  $\omega_j$ . The temperature dependencies of  $C_m(T, B)$  obtained in accordance with Eq. (7) are shown in Fig. 5(b). Near Néel temperature  $T_N(B) \leq 7.4$  K, curves  $C_m(T, B)$  demonstrate a stepwise rise [22,23] (not shown in Fig. 5) whose amplitude steeply decreases with the magnetic field. In the paramagnetic state the  $C_m(T, B)$  plots exhibit a broad peak centered at  $\sim 50$  K [Fig. 5(b)], which corresponds to the magnetic contribution of the holmium subsystem from the excited CF levels. At low temperatures, an additional maximum appears on  $C_m(T, B)$  curves, which may be attributed to a Zeeman-type Schottky anomaly in the heat capacity. To shed more light on the magnetic field effect on heat capacity, field induced differences

$$\Delta C(T, B) = C(T, B) - C(T, B = 0) \quad (9)$$

were introduced, and the corresponding plots are presented in Fig. 6(a). The temperature dependencies of  $\Delta C(T, B)$  demonstrate a wide maximum at about  $T_{\text{max}}^C \approx 12$  K; the maximum amplitude increases strongly with magnetic field [see inset in Fig. 6(a)]. Only very weak decrease of  $T_{\text{max}}^C(B)$  observed in Fig. 6(a) agrees qualitatively with the marked above reduction of holmium magnetic moments and, correspondingly, of Zeeman splittings of CF levels (see also inset in Fig. 3). Short-range order effects playing important role in this reduction were also detected in  $\text{HoB}_{12}$  in Refs. [22–24,33,42,43].

We would like to note that the analysis of field-induced differences  $\Delta C(T, B)$  allowed us to detect an additional fine effect in the heat capacity of  $\text{HoB}_{12}$ . Indeed, a large-scale presentation of  $\Delta C(T, B)$  in the range 40–80 K demonstrates the cage-glass transition at  $T^* \sim 60$  K, which is accompanied by a steplike anomaly for  $\mathbf{B} \parallel [001]$  and  $\mathbf{B} \parallel [110]$ , i.e., in magnetic fields transverse to the cigar-shaped AFM-correlated regions [23], but such a singularity is absent in fields along the [111] direction [see Fig. 6(b)].

The calculated temperature dependence of the molar heat capacity of the subsystem of noninteracting  $\text{Ho}^{3+}$  ions in the cubic CF [the lowest dashed line in Fig. 5(b)] reproduces

satisfactorily the zero-field experimental curve  $C_m(T, 0)$  in the range 30–150 K, but at low temperatures, the results of calculations are remarkably underestimated because of neglected random lattice strains and low-energy excitations with a continuous spectrum originating from magnetic dipole and exchange interactions. In the framework of the dimer model introduced above, the heat capacity is determined by the following expression:

$$C_m(T, B) = \frac{N_A}{2k_B T^2} [\langle H_D^2 \rangle - \langle H_D \rangle^2], \quad (10)$$

where  $N_A$  is the Avogadro number, angular brackets denote the quantum statistical averaging over the canonical ensemble, and  $H_D$  is the dimer Hamiltonian in Eq. (4). The results of calculations for  $\mathbf{B} = 0$  [see line and symbol curve in Fig. 5(b)], where we have employed the CF parameters and the exchange integral obtained from modeling the INS spectra and the low-temperature magnetization, agree substantially better with the experimental curve but remain underestimated.

The detailed theoretical analysis of low-energy excitations in  $\text{HoB}_{12}$  is out of the scope of this paper. To describe the low-temperature behavior of heat capacity, we used the phenomenological approach keeping the dimer model but, having in mind the increasing role of AFM interactions in external magnetic fields which align magnetic moments of neighboring  $\text{Ho}^{3+}$  ions, with varying (increasing with magnetic field) values of the exchange integral and the corresponding mean field constant  $\lambda$ . The satisfactory fitting was achieved by making use of the measured average magnetic moments  $\langle \mathbf{M}(T, \mathbf{B}) \rangle$  of  $\text{Ho}^{3+}$  ions [see Fig. 4(b)] and the exchange integrals  $J_{\text{ex}} = -3.0$  K ( $B = 0$  and 2 T),  $-3.9$  K ( $B = 4$  T),  $-4.3$  K ( $B = 6$  T), and  $-4.4$  K ( $B = 8$  T). The calculated differences  $\Delta C_m(T, B) = C_m(T, B) - C_m(T, 0)$  are compared with the measured ones  $\Delta C(T, B)$  for  $B = 2, 4, 6,$  and  $8$  T in Fig. 6(a). The systematic discrepancies between the results of modeling and the experimental data at temperatures below  $\sim 12$  K point to a possible temperature dependence (enhances with decreasing temperature) of the exchange

integral in the fixed external magnetic field. It should be noted that the obtained strong increase of absolute values of the exchange integral with external magnetic field may be caused, at least partly, by neglecting the magnetic correlations between holmium dimers when fitting the heat capacity curves in Fig. 6(a) by Eq. (10). Also, considering the loosely bound state of  $\text{Ho}^{3+}$  ions in the rigid covalent boron network of  $\text{HoB}_{12}$  and the appearance of dynamic charge stripes along the [110] direction below  $T^* \sim 60$  K, it could be assumed that a significant decrease in the Ho-Ho distance in dimers is induced by a strong external magnetic field, and this assumption should be tested in future experiments.

## VI. CONCLUSIONS

To summarize, the strongly correlated electron system  $\text{Ho}^{11}\text{B}_{12}$  with Jahn-Teller instability of rigid boron network and dynamic charge stripes was studied in detail by INS, magnetometry, and heat capacity measurements at temperatures in the range 3–300 K.

The CF parameters  $B_4 = -0.333$  meV and  $B_6 = -2.003$  meV for  $\text{Ho}^{3+}$  ions in the cubic CF were obtained from the analysis of INS spectra, and the absolute value of  $B_4$  turned out to be significantly lower than the values determined earlier in other magnetic RE (erbium and thulium) dodecaborides. The large ratio  $B_6/B_4$  indicates probably the

dominant contribution of conduction electrons to the CF potential. At temperatures below 30 K, short-range order effects have been found in INS spectra in combination with specific field and temperature dependencies of the low-temperature magnetization and heat capacity which may be discussed in terms of formation below  $T^* \sim 60$  K of holmium dimers in the paramagnetic state of  $\text{HoB}_{12}$  with the cage-glass structure. The MF in the AFM state  $B_{\text{MF}} = (1.75 \pm 0.1)$  T has been determined by fitting the INS spectra at 3.5 K, assuming that the CF parameters are the same as in the paramagnetic phase.

The determination of the magnetic structure of  $\text{HoB}_{12}$  in the magnetically ordered phase remains a challenging problem.

## ACKNOWLEDGMENTS

The work in Prokhorov General Physics Institute of RAS was supported by the Russian Science Foundation, Project No. 17-12-01426, Russian Foundation for Basic Research, Project No. 18-02-01152, and partly performed using the equipment of the Center of Excellence, Slovak Academy of Sciences. The work of K.F., S.G., M.R., and K.S. was supported by the Projects No. APVV-17-0020, No. DAAD-57561069, and VA SR ITMS2014+313011W856. B.Z.M. acknowledges the support by the Russian Science Foundation, Project No. 19-12-00244. The authors are grateful to S. V. Demishev and V. V. Glushkov for helpful discussions.

- 
- [1] N. E. Sluchanko, A. N. Azarevich, A. V. Bogach, I. I. Vlasov, V. V. Glushkov, S. V. Demishev, A. A. Maksimov, I. I. Tartakovskii, E. V. Filatov, K. Flachbart, S. Gabani, V. B. Filippov, N. Y. Shitsevalova, and V. V. Moshchalkov, Effects of disorder and isotopic substitution in the specific heat and Raman scattering in  $\text{LuB}_{12}$ , *JETP* **113**, 468 (2011).
- [2] G. Akopov, M. T. Yeung, and R. B. Kaner, Rediscovering the crystal chemistry of borides, *Adv. Mater.* **29**, 1604506 (2017).
- [3] N. Shitsevalova, Crystal chemistry and crystal growth of rare-earth borides, in *Rare-Earth Borides*, edited by D. S. Inosov (Jenny Stanford Publishing, Singapore, 2022), Chap. 1, pp. 1–243.
- [4] N. E. Sluchanko, A. V. Bogach, V. V. Glushkov, S. V. Demishev, K. S. Lyubshov, D. N. Sluchanko, A. V. Levchenko, A. B. Dukhnenko, V. B. Filipov, S. Gabani, and K. Flachbart, Antiferromagnetic instability and the metal-insulator transition in  $\text{Tm}_{1-x}\text{Yb}_x\text{B}_{12}$  rare earth dodecaborides, *JETP Lett.* **89**, 256 (2009).
- [5] A. Czopnik, N. Shitsevalova, A. Krivchikov, V. Pluzhnikov, Y. Paderno, and Y. Onuki, Thermal properties of rare earth dodecaborides, *J. Solid State Chem.* **177**, 507 (2004).
- [6] F. Iga, N. Shimizu, and T. Takabatake, Single crystal growth and physical properties of Kondo insulator  $\text{YbB}_{12}$ , *J. Magn. Magn. Mater.* **177-181**, 337 (1998).
- [7] F. Iga, Y. Takakuwa, T. Takahashi, M. Kasaya, T. Kasuya, and T. Sagawa, XPS study of rare-earth dodecaborides— $\text{TmB}_{12}$ ,  $\text{YbB}_{12}$ , and  $\text{LuB}_{12}$ , *Solid State Commun.* **50**, 903 (1984).
- [8] T. S. Altshuler, A. E. Altshuler, and M. S. Bresler, An EPR study of the temperature dependence of the energy gap in ytterbium dodecaboride, *JETP* **93**, 111 (2001).
- [9] K. Hagiwara, Y. Takeno, Y. Ohtsubo, R. Yukawa, M. Kobayashi, K. Horiba, H. Kumigashira, J. Rault, P. Le Fèvre, and F. Bertran, Temperature dependence of Yb valence in the sub-surface of  $\text{YbB}_{12}(001)$ , *J. Phys.: Conf. Ser.* **807**, 012003 (2017).
- [10] J. Otsuki, H. Kusunose, P. Werner, and Y. Kuramoto, Continuous-time quantum Monte Carlo method for the Coqblin-Schrieffer model, *J. Phys. Soc. Jpn.* **76**, 114707 (2007).
- [11] A. Akbari, P. Thalmeier, and P. Fulde, Theory of Spin Exciton in the Kondo Semiconductor  $\text{YbB}_{12}$ , *Phys. Rev. Lett.* **102**, 106402 (2009).
- [12] A. F. Barabanov and L. A. Maksimov, Spin excitations in Kondo insulator  $\text{YbB}_{12}$ , *Phys. Lett. A* **373**, 1787 (2009).
- [13] F. Lu, J. Z. Zhao, H. M. Weng, Z. Fang, and X. Dai, Correlated Topological Insulators with Mixed Valence, *Phys. Rev. Lett.* **110**, 096401 (2013).
- [14] H. M. Weng, J. Z. Zhao, Z. J. Wang, Z. Fang, and X. Dai, Topological Crystalline Kondo Insulator in Mixed Valence Ytterbium Borides, *Phys. Rev. Lett.* **112**, 016403 (2014).
- [15] K. Hagiwara, Y. Ohtsubo, M. Matsunami, S. Ideta, K. Tanaka, H. Miyazaki, J. E. Rault, P. Le Fèvre, F. Bertran, A. Taleb-Ibrahimi, R. Yukawa, M. Kobayashi, K. Horiba, H. Kumigashira, K. Sumida, T. Okuda, F. Iga, and S. Kimura, Surface Kondo effect and non-trivial metallic state of the Kondo insulator  $\text{YbB}_{12}$ , *Nat. Commun.* **7**, 12690 (2016).
- [16] N. Sluchanko, A. Bogach, N. Bolotina, V. Glushkov, S. Demishev, A. Dudka, V. Krasnorussky, O. Khrykina, K. Krasikov, V. Mironov, V. B. Filipov, and N. Shitsevalova, Rattling mode and symmetry lowering resulting from the instability of the  $\text{B}_{12}$  molecule in  $\text{LuB}_{12}$ , *Phys. Rev. B* **97**, 035150 (2018).

- [17] N. B. Bolotina, A. P. Dudka, O. N. Khrykina, V. N. Krasnorussky, N. Y. Shitsevalova, V. B. Filipov, and N. E. Sluchanko, The lower symmetry electron-density distribution and the charge transport anisotropy in cubic dodecaboride  $\text{LuB}_{12}$ , *J. Phys.: Condens. Matter* **30**, 265402 (2018).
- [18] N. B. Bolotina, A. P. Dudka, O. N. Khrykina, V. V. Glushkov, A. N. Azarevich, V. N. Krasnorussky, S. Gabani, N. Y. Shitsevalova, A. V. Dukhnenko, V. B. Filipov, and N. E. Sluchanko, On the role of isotopic composition in crystal structure, thermal and charge-transport characteristics of dodecaborides  $\text{Lu}^N\text{B}_{12}$  with the Jahn-Teller instability, *J. Phys. Chem. Sol.* **129**, 434 (2019).
- [19] N. E. Sluchanko, A. N. Azarevich, A. V. Bogach, N. B. Bolotina, V. V. Glushkov, S. V. Demishev, A. P. Dudka, O. N. Khrykina, V. B. Filipov, N. Y. Shitsevalova, G. A. Komandin, A. V. Muratov, Y. A. Aleshchenko, E. S. Zhukova, and B. P. Gorshunov, Observation of dynamic charge stripes in  $\text{Tm}_{0.19}\text{Yb}_{0.81}\text{B}_{12}$  at the metal-insulator transition, *J. Phys.: Condens. Matter* **31**, 065604 (2019).
- [20] B. P. Gorshunov, E. S. Zhukova, G. A. Komandin, V. I. Torgashev, A. V. Muratov, Y. A. Aleshchenko, S. V. Demishev, N. Y. Shitsevalova, V. B. Filipov, and N. E. Sluchanko, Collective infrared excitation in  $\text{LuB}_{12}$  cage-glass, *JETP Lett.* **107**, 100 (2018).
- [21] A. L. Khoroshilov, V. N. Krasnorussky, K. M. Krasikov, A. V. Bogach, V. V. Glushkov, S. V. Demishev, N. A. Samarin, V. V. Voronov, N. Y. Shitsevalova, V. B. Filipov, S. Gabani, K. Flachbart, K. Siemensmeyer, S. Y. Gavrilkina, and N. E. Sluchanko, Maltese cross anisotropy in  $\text{Ho}_{0.8}\text{Lu}_{0.2}\text{B}_{12}$  antiferromagnetic metal with dynamic charge stripes, *Phys. Rev. B* **99**, 174430 (2019).
- [22] K. Krasikov, V. Glushkov, S. Demishev, A. Khoroshilov, A. Bogach, V. Voronov, N. Shitsevalova, V. Filipov, S. Gabani, K. Flachbart, K. Siemensmeyer, and N. Sluchanko, Suppression of indirect exchange and symmetry breaking in the antiferromagnetic metal  $\text{HoB}_{12}$  with dynamic charge stripes, *Phys. Rev. B* **102**, 214435 (2020).
- [23] K. Siemensmeyer, K. Habicht, T. Lonkai, S. Mat'as, S. Gabani, N. Shitsevalova, E. Wulf, and K. Flachbart, Magnetic properties of the frustrated fcc—antiferromagnet  $\text{HoB}_{12}$  above and below  $T_N$ , *J. Low Temp. Phys.* **146**, 581 (2007).
- [24] I. Natkaniec, D. Chudoba, L. Hetmańczyk, V. Yu, J. Kazimirov, and I. L. Krawczyk, Sashin parameters of the NERA spectrometer for cold and thermal moderators of the IBR-2 pulsed reactor, *J. Phys.: Conf. Ser.* **554**, 012002 (2014).
- [25] I. V. Kalinin, V. M. Morozov, A. G. Novikov, A. V. Puchkov, V. V. Savostin, V. V. Sudarev, A. P. Bulkin, S. I. Kalinin, V. M. Pusenkov, and V. A. Ul'yanov, Characteristics of the DIN-2PI spectrometer with a neutron concentrator, *Tech. Phys.* **59**, 307 (2014).
- [26] O. N. Khrykina, A. P. Dudka, N. B. Bolotina, N. E. Sluchanko, and N. Yu. Shitsevalova, Structural instability and poorly defined phase transitions in rare-earth dodecaborides  $\text{RB}_{12}$  ( $R=\text{Ho-Lu}$ ) at intermediate temperatures, *Solid State Sciences* **107**, 106273 (2020).
- [27] N. B. Bolotina, A. P. Dudka, O. N. Khrykina, and V. S. Mironov, Crystal structures of dodecaborides: Complexity in simplicity, in *Rare-Earth Borides*, edited by D. S. Inosov (Jenny Stanford Publishing, Singapore, 2022), Chap. 3, pp. 293–330.
- [28] W. T. Carnall, G. L. Goodman, K. Rajnak, and R. S. Rana, A systematic analysis of the spectra of the lanthanides doped into single crystal  $\text{LaF}_3$ , *J. Chem. Phys.* **90**, 3443 (1989).
- [29] D. S. Pytalev, E. P. Chukalina, M. N. Popova, G. S. Shakurov, B. Z. Malkin, and S. L. Korableva, Hyperfine interactions of  $\text{Ho}^{3+}$  ions in  $\text{KY}_3\text{F}_{10}$ : Electron paramagnetic resonance and optical spectroscopy studies, *Phys. Rev. B* **86**, 115124 (2012).
- [30] A. Abragam and B. Bleaney, *Electron Paramagnetic Resonance of Transition Ions* (Clarendon, Oxford, 1970).
- [31] P. Fulde and M. Loewenhaupt, Magnetic excitations in crystal-field split  $4f$  systems, *Adv. Phys.* **34**, 589 (1985).
- [32] M. A. H. McCausland and I. S. Mackenzie, Nuclear magnetic resonance in rare earth metals, *Adv. Phys.* **28**, 305 (1979).
- [33] M. I. Gilmanov, S. V. Demishev, B. Z. Malkin, A. N. Samarin, N. Yu. Shitsevalova, V. B. Filipov, and N. E. Sluchanko, Electron paramagnetic resonance in  $\text{Ho}_x\text{Lu}_{1-x}\text{B}_{12}$  dodecaborides, *JETP Lett.* **110**, 266 (2019).
- [34] P. A. Alekseev, J.-M. Mignot, K. S. Nemkovski, E. V. Nefeodova, N. Yu. Shitsevalova, Yu. B. Paderno, R. I. Bewley, R. S. Eccleston, E. S. Clementyev, V. N. Lazukov, I. P. Sadikov, and N. N. Tiden, Yb-Yb correlations and crystal-field effects in the Kondo insulator  $\text{YbB}_{12}$  and its solid solutions, *J. Phys.: Condens. Matter* **16**, 2631 (2004).
- [35] P. A. Alekseev, K. S. Nemkovski, J.-M. Mignot, E. S. Clementyev, A. S. Ivanov, S. Rols, R. I. Bewley, V. B. Filipov, and N. Yu. Shitsevalova, Possible undercompensation effect in the Kondo insulator  $(\text{Yb, Tm})\text{B}_{12}$ , *Phys. Rev. B* **89**, 115121 (2014).
- [36] E. A. Goremychkin and E. Myule, Conduction-electron contribution to the crystal potential in intermetallic compounds of rare-earth metals, *JETP Lett.* **39**, 570 (1984).
- [37] N. E. Sluchanko (private communications).
- [38] N. E. Sluchanko, A. L. Khoroshilov, A. V. Bogach, S. Yu. Gavrilkina, V. V. Glushkov, S. V. Demishev, V. N. Krasnorussky, N. Yu. Shitsevalova, V. B. Filipov, S. Gabani, K. Flachbart, and B. Z. Malkin, Magnetic anisotropy of the low-temperature specific heat of  $\text{Ho}_{0.01}\text{Lu}_{0.99}\text{B}_{12}$  with dynamic charge stripes, *JETP Lett.* **108**, 454 (2018).
- [39] S. Gabani, K. Flachbart, K. Siemensmeyer, and T. Mori, Magnetism and superconductivity of rare earth borides, *J. Alloy. Comp.* **821**, 153201 (2020).
- [40] B. Z. Malkin, S. L. Bud'ko, and V. V. Novikov, Crystal-field approach to rare-earth higher borides: Dimerization, thermal, and magnetic properties of  $\text{RB}_{50}$  ( $R = \text{Tb, Dy, Ho, Er, Tm}$ ), *Phys. Rev. Materials* **4**, 054409 (2020).
- [41] N. B. Bolotina (private communication).
- [42] K. M. Krasikov, A. V. Bogach, A. D. Bozhko, V. V. Glushkov, S. V. Demishev, A. L. Khoroshilov, N. Yu. Shitsevalova, V. Filipov, S. Gabani, K. Flachbart, and N. E. Sluchanko, Anisotropy of the charge transport in  $\text{Ho}^{11}\text{B}_{12}$  antiferromagnet with dynamic charge stripes, *Solid State Sci.* **104**, 106253 (2020).
- [43] N. E. Sluchanko, Magnetism, quantum criticality, and metal-insulator transitions in  $\text{RB}_{12}$ , in *Rare-Earth Borides*, edited by D. S. Inosov (Jenny Stanford Publishing, Singapore, 2022), Chap. 4, pp. 331–442.